The Journal of Antibiotics
https://doi.org/10.1038/s41429-020-0293-6

JARA Japan Antibiotics Research Association
The Society for Actinomycetes Japan

ARTICLE

Improvement of the novel inhibitor for *Mycobacterium* enoyl-acyl carrier protein reductase (InhA): a structure–activity relationship study of KES4 assisted by in silico structure-based drug screening

Junichi Taira[1] · Tomohiro Umei[1] · Keitaro Inoue[1] · Mitsuru Kitamura[2] · Francois Berenger[1] · James C. Sacchettini[3] · Hiroshi Sakamoto[1] · Shunsuke Aoki[1]

Received: 28 November 2019 / Revised: 9 January 2020 / Accepted: 10 February 2020

Abstract

InhA or enoyl-acyl carrier protein reductase of *Mycobacterium tuberculosis* (mtInhA), which controls mycobacterial cell wall construction, has been targeted in the development of antituberculosis drugs. Previously, our in silico structure-based drug screening study identified a novel class of compounds (designated KES4), which is capable of inhibiting the enzymatic activity of mtInhA, as well as mycobacterial growth. The compounds are composed of four ring structures (A–D), and the MD simulation predicted specific interactions with mtInhA of the D-ring and methylene group between the B-ring and C-ring; however, there is still room for improvement in the A-ring structure. In this study, a structure–activity relationship study of the A-ring was attempted with the assistance of in silico docking simulations. In brief, the virtual chemical library of A-ring-modified KES4 was constructed and subjected to in silico docking simulation against mtInhA using the GOLD program. Among the selected candidates, we achieved synthesis of seven compounds, and the bioactivities (effects on InhA activity and mycobacterial growth and cytotoxicity) of the synthesized molecules were evaluated. Among the compounds tested, two candidates (compounds **3d** and **3f**) exhibited superior properties as mtInhA-targeted anti-infectives for mycobacteria than the lead compound KES4.

Introduction

Tuberculosis (TB), which is caused by *Mycobacterium tuberculosis*, is one of the most common and serious infectious diseases in the world [1–4]. Multiple drug combination therapy (e.g., isoniazid (INH), rifampicin, ethambutol, and pyrazinamide) has generally been applied in TB treatment to prevent the development of drug resistance; however, inappropriate and/or long-term drug treatment has allowed the emergence of multidrug-resistant TB (MDR-TB) and extensively drug-resistant TB (XDR-TB). Treatment for MDR-TB and XDR-TB is long, expensive, and characterized by a high rate of adverse events. The main difficulty is the identification of at least four active drugs in order to design an effective regimen [5]. It is therefore imperative to develop a novel class of anti-infectives capable of sterilizing drug-resistant mycobacteria.

The enoyl-acyl carrier protein reductase (InhA, EC 1.3.1.9) is known to be involved in the biosynthesis of mycolic acids, a major component of mycobacterial cell walls. The compounds capable of inhibiting enzymatic activity of *M. tuberculosis* InhA (mtInhA) have been developed as anti-TB drugs [6–9]. Indeed, mtInhA is the primary target of the first-line antitubercular drug INH and of the second-line drug ethionamide (ETH). The enzyme catalyzes the NADH-dependent reduction of the double bond of 2-trans-enoyl-acyl carrier protein, an essential step in the fatty acid elongation cycle of the type II fatty acid synthase (FAS-II) system, which is significantly different to the mammalian fatty acid synthesis pathway [10–13]. INH and ETH inhibit InhA by covalently bonding to NAD at the active site of

Supplementary information The online version of this article (https://doi.org/10.1038/s41429-020-0293-6) contains supplementary material, which is available to authorized users.

✉ Shunsuke Aoki
aokis@bio.kyutech.ac.jp

[1] Department of Bioscience and Bioinformatics, Graduate School of Computer Science and Systems Engineering, Kyushu Institute of Technology, Iizuka 820-8502, Japan

[2] Department of Applied Chemistry, Kyushu Institute of Technology, 1-1 Sensui-cho, Tobata, Kitakyushu 804-8550, Japan

[3] Department of Biochemistry & Biophysics, Texas A&M University, College Station, TX 77843-2128, USA

Published online: 09 March 2020

mtInhA. Although many INH- and ETH-resistant clinical isolates contain mutations within the *inhA* locus, resistance can be conferred by mutation(s) at Ile21, Ile47, or Ser94 [14].

We have previously demonstrated that in silico structure-based drug screening (SBDS) is suitable for screening lead compounds of novel enzyme inhibitors and is a promising tool that offers cost- and labor-saving advantages over the use of random high-throughput screening methods [15–19]. A series of KES compounds, which contain 3-(phenoxy) benzylpiperazine pharmacophore, has been identified, with the assistance of in silico SBDS, as being inhibitory to mtInhA [17]. Among the compounds tested, KES4: 1-(2-furoyl)-4-{3-(phenoxy)benzyl}piperazine exhibited a potent inhibition of mycobacterial growth, which appears to be associated with InhA inhibition. As shown in Fig. 1, KES4 is composed of two phenyl, piperazinyl, and furoyl groups (the ring structures are referred to as the A–D-rings). Our previous simulation presumed that the 2-furoyl group and its oxygen atom (D-ring) were involved in hydrophobic interactions with Leu218 and hydrogen bonding with Tyr158, respectively [17]. The hydrogen atom on methylene, between the piperazinyl group (C-ring) and the 3-phenoxybenzyl group (B-ring), interacts with Phe149 by a CH-π interaction. Since Phe149, Tyr158, and Leu218 are located in the active site of mtInhA, the B–D-rings play important roles in mtInhA inhibition, although specific interactions were not predicted on the A-rings. The simulation suggested that the compound can still be improved.

A conventional structure–activity relationship (SAR) study, based on minor modifications of the lead compounds, is an orthodox strategy for obtaining KES4-based novel effective InhA inhibitors, although this requires deep insights into protein–molecule interactions, as well as synthesis of many compounds. The in silico SBDS technique is one of the powerful tool to find lead compounds with novel pharmacophore; however, related molecular selection, on the basis of the matched molecular pair (MMP) method [19], is dependent on the scale of the chemical library used, i.e., commercially unavailable compounds are excluded from the selection because chemical libraries have generally been constructed based on commercially available (known) compounds. Thus, to overcome these issues, a tailored chemical library of A-ring-modified KES4 derivatives was prepared and subjected to in silico docking simulation in this study.

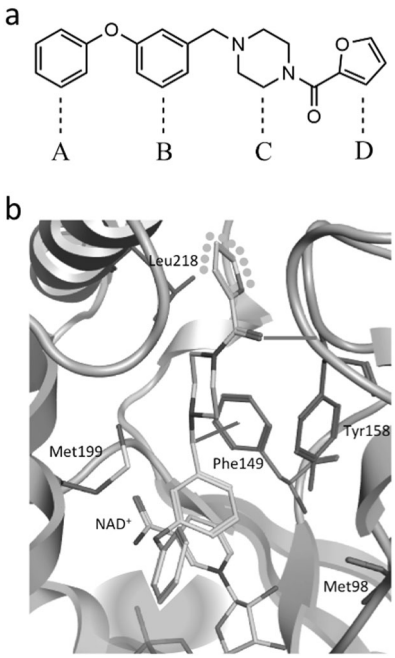

Fig. 1 Chemical structures of KES4 and predicted interaction with mtInhA. **a** Chemical structure of KES4. The phenyl and heterocyclic rings are referred to as A–D-rings. **b** Predicted interactions of KES4 (light blue) to active site of mtInhA (gray): where the blue lines between the methylene (between the C-ring and B-ring) and the Phe149 indicates CH–π interaction; the orange dots surrounding the 2-furoyl group of indicates hydrophobic interactions with the Leu218; the green line between the D-ring proximal carbonyl group and the Tyr158 indicates hydrogen bond; the red shaded area represents gap between the A-ring and the enzyme

Experimental procedure

Preparation of the compound library and protein structural data

A total of 243 commercially available phenol analogs (with >70% structural similarity to phenol) were selected from the PubChem database (https://pubchem.ncbi.nlm.nih.gov/), and a chemical library of KES4 derivatives was generated using the canonical SMILES notation. Conversion to MOL2-formatted three-dimensional chemical structures, the addition of hydrogen atoms and electric charges, and structural optimization were performed using the Energy Minimize, Protonate 3D, and Energy Minimize modules, respectively, which have been implemented in the Molecular Operating Environment (MOE) version 2011.10 (Chemical Computing Group, Montreal, Canada). In general, to screen for a competitive inhibitor using the SBDS strategy, the utilization of substrate- or inhibitor-bound forms of protein structures is preferable to apo-form structures. The protein data bank (PDB) structural data of mtInhA in complex with pyrrolidine carboxamide derivative (PDB-id 4U0J) [20] was therefore employed in the present SBDS after following structural adjustments. In brief, hydrogen atoms and electric charges were added using the Protonate 3D module in the MOE software after the removal of water, oxygen atoms, and the pyrrolidine carboxamide-derived inhibitor from the structure. Then, hydrogen atoms were optimized with the Energy Minimize module in MOE software.

In silico docking simulation

Binding affinity between the 243 compounds in the chemical library and the mtInhA substrate-binding cavity was predicted using tandem (two-step) GOLD screening with Cambridge Crystallographic Data Center GOLD suite version 5.3 [15–18, 21, 22]. The primary screening of the compounds with single conformations identified 209 compounds with a GOLD score above that of KES4 (81.80). Then, ten conformations of each compound were generated by the Conformation Search module of MOE and were subjected to secondary screening. As the result of the secondary screening, 199 compounds with a GOLD score above that of KES4 (80.36 ± 1.57) were identified. Binding between the compounds and amino acids, constituting the mtInhA substrate-binding cavity, was presumed by ligand interaction (LI) and protein–ligand interaction fingerprint (PLIF) modules in MOE software. According to the LI and PLIF results, the compounds that could interact with Phe149, Thr158, and Leu218 of mtInhA were kept as candidates, although those which could interact with Ile21, Ile47, or Ser94 were excluded. Sixteen candidate compounds were selected and designated as KET1-16 (Fig. S1). We also predicted the toxicity of the compounds (Fig. S2). Classification Quantitative Structure–Activity Relationship (classification QSAR) models were trained on the Toxicology in the 21st Century (Tox21) dataset [23]. Tox21 contains toxicity data for 12 toxicity end-points (NR-AR, NR-AR-LBD, NR-AhR, NR-Aromatase, NR-ER, NR-ER-LBD, NR-PPAR-gamma, SR-ARE, SR-ATAD5, SR-HSE, SR-MMP, and SR-p53) and ~8000 ligands. We standardized all molecules using Francis Atkinson's standardizer (https://github.com/flatkinson/standardiser). Molecules were then encoded using Faulon's signature molecular descriptor [24], with height one bond and parameterized over MOL2 atom types. Our molecular encoder is released as open-source [25]. For each target, only molecules tested as toxic or nontoxic on that target were retained. Not all Tox21 molecules have a toxicity outcome against all targets. We then trained a classification QSAR model on each target. Each model consists in a bag [26] of 11 linear support vector machines (R package svmpath; dot product kernel) trained on balanced bootstraps. Each model had an AUC between 0.75 and 0.85. However, the models for SR-ATAD5 and NR-Aromatase did not show a good separation of the predicted scores between toxic and nontoxic molecules, so their predictions might be inaccurate. Finally, for each target, a toxicity probability model (Eq. (1)) was fitted with gnuplot using five folds cross validation when training each QSAR model. This probability model allows the transformation of raw scores from each QSAR model into toxicity probabilities. The final production QSAR models were trained using all data for each Tox21 target. The logistic curve was used for the toxicity probability model (a and b are the two parameters adjusted upon fitting). This method is called Platt scaling [27]. The "x" is the raw toxicity score given by a classification model for a given candidate molecule.

$$p\_\{\text{toxic}\}(x) = 1.0/(1.0 + \exp(a \times x + b)). \quad (1)$$

Regarding Fig. S2, several compounds look quite safe across all Tox21 toxicity end-points: KES4, KES3, KET1, KET12, and KET8. Some other compounds have a warning regarding a possible effect on the mitochondrial function (stress response pathway mitochondrial membrane potential —SR-MMP in Tox21). Those compounds are: KES5, KET13, KET4, KET5, and KET7.

Chemistry and chemical methods

The general synthetic scheme employed in this study is illustrated in Fig. 2. All reagents and solvents were commercially available and required no further purification. All reactions were carried out under nitrogen or argon. All compounds were purified by silica gel column chromatography (Fuji Silysia Silica gel PSQ-100B or Kanto Chemical Silica Gel 60N). NMR spectra were recorded on a Bruker Avance 500 system (Bruker) in $CDCl_3$ [TMS (for 1H, $\delta = 0$) or $CDCl_3$ (for 13C, $\delta = 77.0$) was used as an internal standard]. Mass spectra were obtained with a JEOL JMS-SX102A mass spectrometer (JEOL) using an electron ionization method with a double focusing sector detector.

General procedure for synthesis of intermediate 3-phenoxybenzaldehyde derivatives 2a–g

Potassium hydroxide (1.2 eq) was added to a solution of phenol derivatives **1a–g** (1.8 eq) in *m*-xylene. The solution was refluxed at 130 °C for 2 h and was then cooled to room temperature. Copper (I) chloride (0.013 eq) and 2-(3-bromophenyl)-1,3-dioxolane (1 eq) were added to the reaction mixture, and stirring continued overnight at 130 °C. The reaction was quenched by the addition of water and then extracted with dichloromethane. The organic layer was washed with brine, and the organic solvent was evaporated under reduced pressure. The residue was redissolved in 1:1 THF/H_2O and 2,2,2-trifluoroacetic acid (1.5 eq). The reaction mixture was then stirred at room temperature for 2 h. The reaction was quenched by an aqueous solution of sodium hydroxide and was then extracted with ethyl acetate. The organic layer was washed with brine and dried with anhydrous Na_2SO_4. The organic solvent was evaporated under reduced pressure to obtain the crude products **2a–g**.

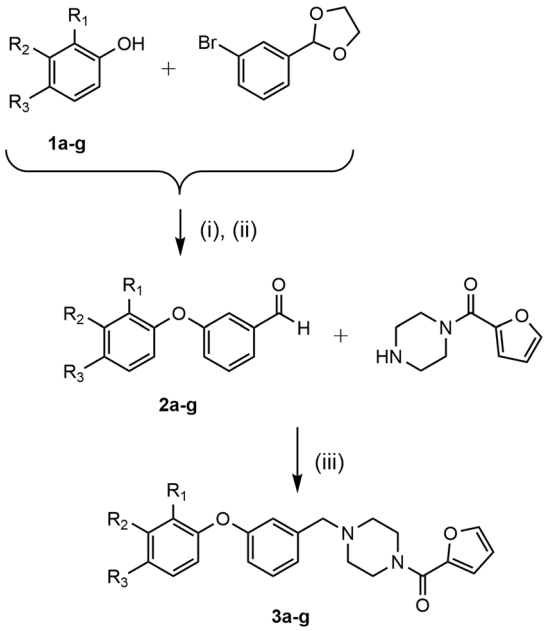

1a, 2a, and 3a:	R_1=H	R_2=H	R_3=CH_2COOCH_3
1b, 2b, and 3b:	R_1=H	R_2=*t*-Bu	R_3=H
1c, 2c, and 3c:	R_1=*s*-Bu	R_2=H	R_3=H
1d, 2d, and 3d:	R_1=Et	R_2=H	R_3=H
1e, 2e, and 3e:	R_1=H	R_2= CF_3	R_3=H
1f, 2f, and 3f:	R_1=Me	R_2=H	R_3=H
1g, 2g, and 3g:	R_1=*t*-Bu	R_2=H	R_3=H

Fig. 2 Synthetic scheme of KES4 related compounds. (i) KOH, *m*-xylene, CuCl (I), 140 °C. (ii) TFA, THF/water (1:1) r.t. (iii) $NaBH(OAc)_3$, CH_2Cl_2, r.t

General procedure for synthesis of the target 1-(2-furoyl)-4-(3-phenoxybenzyl)piperazine derivatives 3a–g

1-(2-Furoyl)piperazine (1.1 eq) and sodium acetoxyborohydride (1.2 eq) were added to a solution of 3-phenoxybenzaldehyde derivatives **2a**–**g** (1 eq) in dichloromethane. The reaction mixture was stirred at room temperature. After overnight stirring, the reaction was quenched by the addition of water and was then extracted with dichloromethane. The organic layer was washed with brine and dried with anhydrous Na_2SO_4. The organic solvent was evaporated under reduced pressure to obtain the crude products **3a**–**g**. The spectral data of compounds **3a**–**g** are reported herein in detail.

Compound 3a (KET1)

(1-(2-furoyl)-4-{3-[4-(methoxycarbonylmethyl)phenoxy] benzyl}piperazine): Yield 92%; ^{1}H NMR (500 MHz, $CDCl_3$) δ 7.46 (1H, s, Ar–H), 7.29–7.23 (3H, m, Ar–H), 7.07 (1H, d, $J = 7.7$ Hz, Ar–H), 7.03 (1H, s, Ar–H), 6.98–6.94 (3H, m, Ar–H), 6.90 (1H, dd, $J = 7.6$, 2.4 Hz, Ar–H), 6.47 (1H, s, Ar–H), 3.80 (4H, s, $CH_2 \times 2$), 3.71 (3H, s, CH_3), 3.61 (2H, s, CH_2), 3.52 (2H, s, CH_2), 2.50 (4H, t, $J = 4.9$ Hz, $CH_2 \times 2$); ^{13}C NMR (126 MHz, $CDCl_3$) δ (ppm) 172.1, 159.0, 157.2, 156.4, 148.0, 143.6, 139.9, 130.6, 129.6, 128.8, 124.0, 119.4, 118.8, 117.7, 116.2, 111.2, 62.5, 53.1, 52.0, 40.4; MS *m/z* (M + H, $C_{25}H_{26}N_2O_5$), found 435.

Compound 3b (KET3)

(1-(2-furoyl)-4-{3-[3-(*tert*-butyl)phenoxy]benzyl}piperazine): Yield 39%; ^{1}H NMR (500 MHz, $CDCl_3$) δ 7.49 (1H, s, Ar–H), 7.26 (2H, q, $J = 8.2$ Hz, Ar–H), 7.14 (1H, d, $J =$ 7.9 Hz, Ar–H), 7.08 (1H, s, Ar–H), 7.05 (1H, d, $J = 3.8$ Hz, Ar–H), 6.97 (1H, d $J = 3.5$ Hz, Ar–H), 6.90 (1H, dd, $J =$ 8.1, 1.7 Hz, Ar–H), 6.79 (1H, dd, $J = 8.0$, 2.4 Hz, Ar–H), 6.47 (1H, s, Ar–H), 3.79 (4H, s, $CH_2 \times 2$), 3.51 (2H, s, CH_2), 2.50 (4H, t, $J = 4.8$ Hz, $CH_2 \times 2$), 1.30 (9H, s, $CH_3 \times$ 3); ^{13}C NMR (126 MHz, $CDCl_3$) δ (ppm) 159.0, 157.5, 153.5, 148.0, 143.6, 139.7, 129.6, 129.2, 123.7, 120.3, 119.2, 117.4, 116.4, 116.3, 115.7, 111.2, 62.5, 34.8, 31.3; MS *m/z* (M + H, $C_{26}H_{30}N_2O_3$), found 419.

Compound 3c (KET6)

(1-(2-furoyl)-4-{3-[2-(*sec*-butyl)phenoxy]benzyl}piperazine): Yield 25%; ^{1}H NMR (500 MHz, $CDCl_3$) δ 7.46 (1H, s, Ar–H), 7.29 (1H, dd, $J = 7.1$, 2.1 Hz, Ar–H), 7.24 (1H, t, $J = 7.9$ Hz, Ar–H), 7.15–7.12 (2H, m, Ar–H), 7.00 (1H, d, $J = 7.7$ Hz, Ar–H), 6.97 (1H, d, $J = 3.5$ Hz, Ar–H), 6.92 (1H, s, Ar–H), 6.88 (1H, dd, $J = 6.8$, 2.2 Hz, Ar–H), 6.81 (1H, dd, $J = 8.2$, 2.5 Hz, Ar–H), 6.47 (1H, s, Ar–H), 3.79 (4H, s, $CH_2 \times 2$), 3.50 (2H, s, CH_2), 2.49 (4H, t, $J = 4.9$ Hz, $CH_2 \times 2$), 1.68–1.53 (3H, m, CH, CH_2), 1.20 (3H, d, $J =$ 7.0, CH_3), 0.82 (3H, t, $J = 7.4$, CH_3); ^{13}C NMR (126 MHz, $CDCl_3$) δ (ppm) 159.1, 158.5, 153.9, 148.0, 143.6, 139.7, 139.1, 129.4, 127.6, 126.8, 124.2, 123.0, 119.8, 118.1, 116.4, 116.2, 111.2, 62.6, 34.0, 30.1, 21.0, 12.3; MS *m/z* (M + H, $C_{26}H_{30}N_2O_3$), found 419.

Compound 3d (KET8)

(1-(2-furoyl)-4-[3-(2-ethylphenoxy)benzyl]piperazine): Yield 43%; ^{1}H NMR (500 MHz, $CDCl_3$,) δ 7.46 (1H, s, Ar–H), 7.29–7.19 (2H, m, Ar–H), 7.16 (1H, dt, $J = 7.7$, 1.6 Hz, Ar–H), 7.10 (1H, dt, $J = 7.4$, 1.3 Hz, Ar–H), 7.01 (1H, d, $J = 7.6$ Hz, Ar–H), 6.97 (1H, d, $J = 3.5$ Hz, Ar–H), 6.94 (1H, s, Ar–H), 6.88 (1H, dd, $J = 8.0$, 1.2 Hz, Ar–H), 6.80 (1H, dd, $J = 8.1$, 2.1 Hz, Ar–H), 6.46 (1H, s, Ar–H), 3.80 (4H, s, $CH_2 \times 2$), 3.50 (2H, s, CH_2), 2.65 (2H, q, $J = 2.5$ Hz, CH_2), 2.49 (4H, t, $J = 4.7$ Hz, $CH_2 \times 2$), 1.20 (3H, t, $J = 7.6$, CH_3); ^{13}C NMR (126 MHz, $CDCl_3$) δ (ppm) 159.1, 158.2, 154.2, 148.0, 143.6, 139.7, 135.8, 131.9, 130.4, 129.9, 129.5, 127.6, 127.1, 124.0, 123.1, 119.6, 118.2, 116.2, 111.2, 62.5, 53.1, 23.2, 14.5; MS *m/z* (M + H, $C_{24}H_{26}N_2O_3$), found 391.

Compound 3e (KET10)

(1-(2-furoyl)-4-{3-[3-(trifluoromethyl)phenoxy]benzyl} piperazine): Yield 42%; ^{1}H NMR (500 MHz, $CDCl_3$) δ 7.46 (1H, s, Ar–H), 7.44 (1H, t, $J = 8.1$, Ar–H), 7.35–7.31 (2H, m, Ar–H), 7.22 (1H, s, Ar–H), 7.17 (1H, dd, $J = 8.2$, 2.2 Hz, Ar–H), 7.13 (1H, d, $J = 7.6$ Hz, Ar–H), 7.06 (1H, s, Ar–H), 6.98 (1H, d, $J = 3.5$ Hz, Ar–H), 6.93 (1H, dd, $J = 7.8$, 1.8 Hz, Ar–H), 6.47 (1H, s, Ar–H), 3.80 (4H, s, $CH_2 \times 2$), 3.54 (2H, s, CH_2), 2.50 (4H, t, $J = 4.6$ Hz, $CH_2 \times 2$); ^{13}C NMR (126 MHz, $CDCl_3$) δ (ppm) 159.1, 157.8, 156.3, 148.0, 143.6, 140.3, 130.3, 129.9, 124.8, 121.6, 119.9, 119.6, 118.2, 116.3, 115.1, 111.2, 62.4, 53.1; MS *m/z* (M + H, $C_{23}H_{21}F_3N_2O_3$), found 431.

Compound 3f (KET12)

(1-(2-furoyl)-4-[3-(2-methylphenoxy)benzyl]piperazine): Yield 46%; ^{1}H NMR (500 MHz, $CDCl_3$) δ 7.46 (1H, s, Ar–H), 7.26–7.19 (2H, m, Ar–H), 7.16 (1H, t, $J = 7.2$ Hz, Ar–H), 7.06 (1H, t, $J = 7.4$ Hz, Ar–H), 7.01 (1H, d, $J = 7.5$ Hz, Ar–H), 6.98 (1H, t, $J = 1.8$ Hz, Ar–H), 6.93 (1H, s, Ar–H), 6.89 (1 H, d, $J = 8.0$ Hz, Ar–H), 6.78 (1H, dd, $J = 8.1$, 2.4 Hz, Ar–H), 6.46 (1H, s, Ar–H), 3.80 (4H, s, $CH_2 \times 2$), 3.50 (2H, s, CH_2), 2.49 (4H, t, $J = 4.7$ Hz, $CH_2 \times 2$), 2.23 (3H, s, CH_3); MS *m/z* (M + H, $C_{23}H_{24}N_2O_3$), found 377.

Compound 3g (KET15)

(1-(2-furoyl)-4-{3-[2-(*tert*-butyl)phenoxy]benzyl}piperazine): Yield 66%; ^{1}H NMR (500 MHz, $CDCl_3$) δ 7.46 (1H, s, Ar–H), 7.40 (1H, dd, $J = 8.3$, 1.7 Hz, Ar–H), 7.26 (1H, t, $J = 7.9$ Hz, Ar–H), 7.13 (1H, td, $J = 7.7$, 1.7 Hz, Ar–H), 7.07–7.03 (2H, m, Ar–H), 6.99–6.97 (2H, m, Ar–H), 6.86 (1H, dd, $J = 7.6$, 1.8 Hz, Ar–H), 6.80 (1H, dd, $J = 8.0$, 1.4 Hz, Ar–H), 6.47 (1H, s, Ar–H), 3.80 (4H, s, $CH_2 \times 2$), 3.52 (2H, s, CH_2), 2.50 (4H, t, $J = 4.7$ Hz, $CH_2 \times 2$), 1.42 (9H, s, $CH_3 \times 3$); ^{13}C NMR (126 MHz, $CDCl_3$) δ (ppm) 159.1, 157.9, 155.8, 148.0, 143.6, 140.9, 139.7, 129.5, 127.2, 127.1, 123.3, 123.2, 120.1, 119.2, 117.5, 116.3, 111.2, 62.5, 53.1, 34.8, 30.1; MS *m/z* (M + H, $C_{26}H_{30}N_2O_3$), found 419.

Antimycobacterial assay

Mycobacterium smegmatis (IAM 12065 strain, RIKEN BioResource Center, Saitama, Japan) was grown at 37 °C for 24 h in 3.7% brain–heart infusion broth (Sigma, St. Louise, MO, USA). Cultures were then diluted 70-fold with broth that contained the candidate compounds in 96-well flat-bottom clear plates (Corning, NY, USA). Each well was inoculated with 150 µl of culture. Isoniazid (INH) (LKT Laboratories, St. Paul, MN, USA) and 0.3% DMSO were used as positive and negative controls, respectively. The plates were incubated at 37 °C for 24 h, and then the cell cultures were subjected to growth inhibition assays. The inhibition of bacterial growth was determined by measuring OD_{595} using a Bio-Rad Model 680 microplate reader (Bio-Rad, Hercules, CA, USA).

Cytotoxic assay

The Madin–Darby canine kidney (MDCK) cell lines were maintained in high-glucose Dulbecco's Modified Eagle Medium (DMEM) supplemented with 10% fetal bovine serum (FBS), 2 mM L-glutamine, 100 U ml^{-1} of penicillin, and 100 µg ml^{-1} of streptomycin and cultured at 37 °C in a humidified atmosphere containing 5% CO_2. The cells (1.5×10^4 cells/well) were seeded into 96-well plates 6 h before serum starvation with 0.25% FBS containing DMEM. After 24 h of serum starvation, the compounds (50 µM) were added. Triclosan (TCS) (50 µM) and DMSO (0.3%) were used as positive and negative controls, respectively. The cultures were incubated for an additional 24 h, and then the cytotoxicity of the compounds was analyzed with a Cell Counting Kit-8 (Dojin, Kumamoto, Japan), as previously described [17].

Assay of mtInhA activity

The detail of cloning, expression, and purification of mtInhA have been reported by Molle et al. [28]. We previously reported the methods not only for synthesizing of trans-2-decenoyl CoA as InhA substrate, but also for determining mtInhA activity based on the technique by Delaine et al. [17, 29]. The recombinant mtInhA briefly, the preincubation of enzyme, and inhibitors was performed in 50 µl (total volume) of 30 mM PIPES (pH 6.8), 150 mM

NaCl, 200 μM NADH, 700 nM mtInhA, and compounds **3a**, **3b**, **3c**, **3d**, **3e**, **3f**, or **3g** (50 μM). DMSO was used as cosolvent, and its final concentration was <0.5%. After 1 min of preincubation at 25.5 °C, the addition of 200 μM substrate (trans-2-decenoyl-CoA) initiated the reaction which was followed at 340 nm (oxidation of NADH) and at 25 °C using an Infinite M200 PRO microplate reader (TECAN, Männedorf, Switzerland). The inhibitory activity of each compound tested was determined based on the absorbances 5 min after the addition of substrate (trans-2-decenoyl-CoA) and was expressed as the percentage of mtInhA activity recorded in the absence of inhibitor.

Results

Identification of candidate compounds by SBDS

We previously reported the identification of KES4, a novel inhibitor of *M. tuberculosis* InhA [17]. Herein, a chemical library composed of 243 A-ring modified KES4 derivatives was prepared and subjected to in silico SBDS to assist in the structural refinement of the KES4 A-ring for mtInhA inhibition. The GOLD program evaluates the binding affinity of compounds to enzyme active sites and provides a GOLD score by calculating protein–ligand hydrogen bonding energy, van der Waals contact energy, and molecule torsion energy based on a genetic algorithm [30, 31]. The tandem GOLD screening strategy, comprised of primary and secondary screenings with single and multiple conformations of compounds, respectively, resulted in the identification of 199 compounds with GOLD scores above than that of KES4 (80.36 ± 1.57). The candidate compounds were further selected on the basis of having specific interactions with amino acids in mtInhA, which were determined by LI and PLIF simulations. Compounds that could interact with Phe149, Tyr158, and Leu218 of mtInhA were presumed to be involved in interactions with KES4 and were kept as candidates, while compounds that could interact with Ile21, Ile47, or Ser94 of mtInhA, which are known to be associated with the acquisition of drug resistance in *M. tuberculosis*, were excluded. The final 16 candidate compounds were referred to as KET1-16, as shown in Fig. S1.

Synthesis of compounds

The synthetic strategy and structures of the KES4 derivatives is shown in Fig. 2. Among the candidate compounds KET1-16, we succeeded in synthesizing KET1, 3, 6, 8 10, 12, and 15. Hereafter, these synthesized compounds are referred to as compounds **3a**–**g**. The other compounds were not obtained in sufficient quantities or adequate levels of purity. It might be better that some phenols with additional OH/NH groups were protected by appropriate protecting groups. Although the reasons for the failures to synthesize the compounds are of interest, we did not investigate these further in this study.

Growth inhibition of M. smegmatis by compounds 3a–g

As a primary evaluation of bioactivity, the effect of compounds **3a**–**g** on mycobacterial growth inhibition was examined. *M. smegmatis* (biosafety level 1) was utilized as a model mycobacteria in the antimycobacterial experiments. *M. smegmatis* InhA shares 87% similarity with mtInhA in amino acid sequence. We also previously confirmed that tertiary structures of these inhibitor binding cavity were comparable [17]. The inhibitory effects on mycobacterial growth of the 50 μM compound solutions are presented in Fig. 3. Compound **3a** showed only ca. 40% growth inhibition, while the other compounds (**3b**–**g**) almost completely inhibited mycobacterial growth. None of the compounds exhibited any significant antimicrobial activity against *Escherichia coli* at a concentration of 100 μM (Fig. S3), suggesting that the compounds had mycobacteria-selective growth inhibitory properties.

Next, we examined the dose dependency of the inhibitory effect (Fig. 4). The concentrations of compounds that exerted a 50% inhibition of *M. smegmatis* growth (IC_{50} values) were as follows: KES4 (lead compound), 9.6 μM; compound **3a**, 26.8 mM; compound **3b**, 1.8 μM; compound **3c**, 2.2 μM; compound **3d**, 3.4 μM; compound **3e**, 22.8 μM; compound **3f**, 7.8 μM; and compound **3g**, 5.0 μM. According to a previous study, the IC_{50} value of isoniazid (the positive control) is 5.4 μM [16].

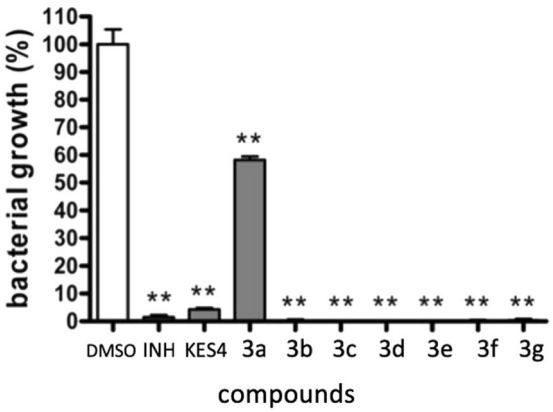

Fig. 3 Antimicrobial activity of the compounds on the growth of *M. smegmatis*. The inhibitory effect on bacterial growth was monitored by OD_{595} at 24 h after treatment with compounds (50 μM). Isoniazid (INH, 50 μM) and 0.3% DMSO were used as positive and negative controls, respectively. All experiments were performed in quadruplicate, and data with error bars are expressed as mean ± SD. Significance was evaluated by Dunnett's test: $^{**}p < 0.001$

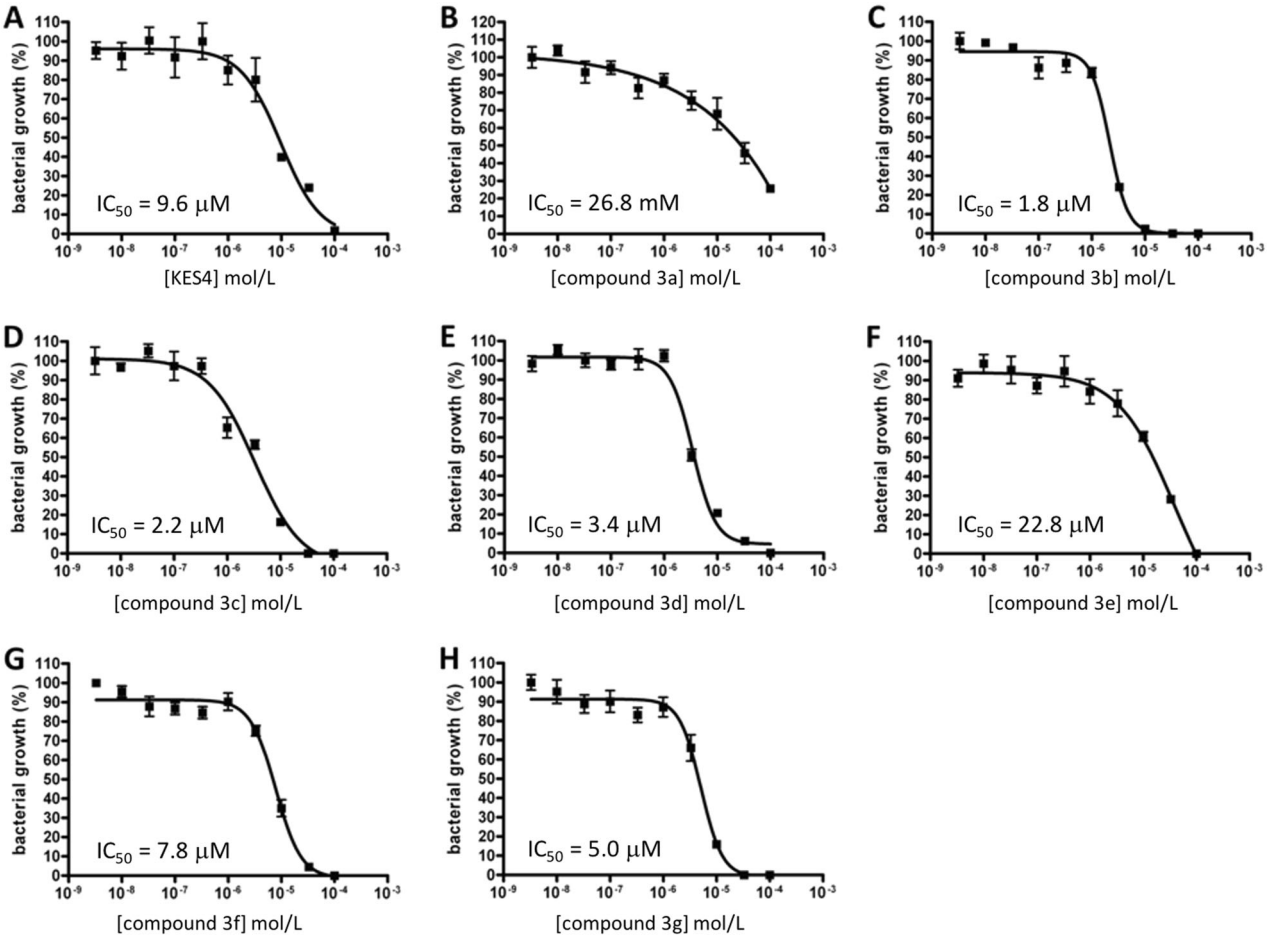

Fig. 4 Dose dependence of the compounds on the growth of *M. smegmatis*: **a** KES4 (as lead compound); **b–h** Compounds **3a–g**. The inhibitory effect on bacterial growth was monitored by OD_{595} at 24 h after treatment with the compounds. All experiments were performed in quadruplicate, and data with error bars are expressed as mean ± SD. IC_{50} values were determined based on a nonlinear regression method

Cytotoxicity of the compounds

To probe the damaging effects of the compounds on mammalian cells, cytotoxicity was measured using the MDCK cell line (Fig. 5). TCS, a representative InhA inhibitor with a diphenyl ether pharmacophore [7, 8], was used as a positive control. Compounds **3a** and **3d–f** did not show a significant cytotoxicity. Compounds **3b** and **3c** showed modest cytotoxicity at 50 μM, and this was comparable with that of TCS.

Effects of compounds 3a–g on the enzymatic activity of mtInhA

The effects of compounds **3a–g** on the enzymatic activity of recombinant mtInhA were examined to evaluate mtInhA inhibition. Parikh et al. reported that TCS inhibits mtInhA with a K_i value of 0.2 μM and, as shown in Fig. 6, mtInhA was almost completely inhibited in the presence of 50 μM TCS [7]. The enzymatic activity of mtInhA was suppressed

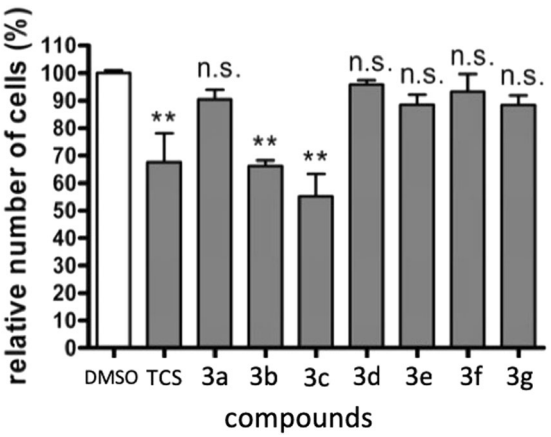

Fig. 5 Cytotoxicity of the compounds against the MDCK cell line. The concentration of the compounds was 50 μM. Triclosan (TCS, 50 μM) and 0.3% DMSO were used as positive and negative controls, respectively. All experiments were performed in quadruplicate, and data with error bars were expressed as mean ± S.D. Cell survival rates were compared using Dunnett's test for significance: $^{**}p < 0.001$

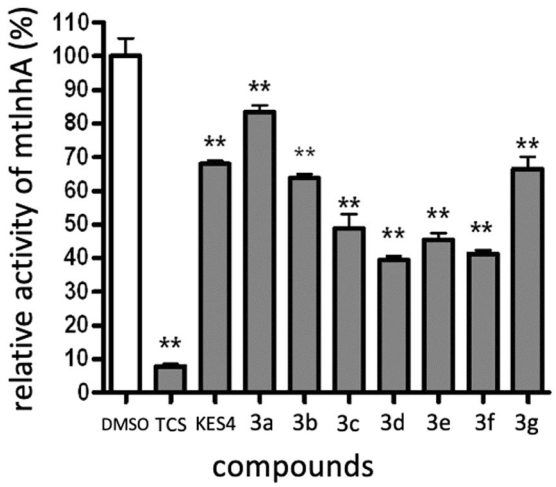

Fig. 6 Effect of compounds on enzymatic activity of mtInhA. The enzymatic activity was measured as described in the experimental procedures. MtInhA (0.7 μM) was preincubated with each compound (50 μM) at room temperature for 1 min before its activity was measured. Triclosan (TCS) and 0.3% DMSO were used as positive and negative controls, respectively. All experiments were performed in quadruplicate, and data with error bars were expressed as mean ± SD

to 68% (32% of the InhA activity was inhibited) in the presence of 50 μM KES4 (Fig. 6 and Table 1). Among the tested compounds, mtInhA activity was suppressed to 39.5% and 41.2% in the presence of compounds **3d** and **3f**, respectively (these compounds inhibited ca. 60% of InhA activity). Inhibitory activity of these compounds was only moderately but more potent than that of KES4.

Discussion

Structural modification of KES4 could provide a novel class of compounds with potent antimycobacterial activity. As described in the previous section, KES4 seems to interact with Leu218, Tyr158, and Phe149 in mtInhA through its B–D-rings [17], while specific interaction was not predicted for the A-ring (Fig. 1b). In this study, to increase the affinity of KES4 for mtInhA, the chemical library constituted by a series of A-ring-modified KES4 was prepared and subjected to docking simulation. We tried to synthesize top 16 compounds selected by the in silico docking simulations, though the synthetic method for KES4 failed to introduce electronegative atoms on the A-rings excepting KET1 (i.e., KET2, KET4, KET5, KET7, KET9, KET13, and KET16). Other synthetic methods have not been tested at present stage due to achievement of synthesis on all compounds was not important issues. Resulting from the in silico docking simulation and successive organic syntheses, we succeeded in obtaining seven candidate compounds.

Compounds **3b**–**g** showed comparable or higher levels of activity in terms of inhibiting *Mycobacterium* growth when compared with the lead compound (KES4), while the introduction of a methoxycarbonylmethyl group (compound **3a** or KET1) on the A-ring abolished the antimycobacterial activity (Figs. 3 and 4). As shown in Table 1, compound **3a** showed highest topological polar surface area and lowest Log*P* values in comparison with KES4 and other candidates. Since the cell wall of *Mycobacterium* is rich in hydrophobic mycolic acid [10, 13], the hydrophilicity of methoxycarbonylmethyl group can exert disadvantageous effect on mycobacterial cell wall permeation among the tested compounds. In addition, mtInhA inhibitory activity of compound **3a** was also lower than that of KES4 (Fig. 6). Combined, both an antimycobacterial and mtInhA inhibitory activity of KES4 could be spoiled by introduction of electronegative atoms to the A-rings. Enzymatic inhibitory potency of the KES4 derivatives also seems to correspond with the size of hydrophobic substituents on the A-ring for the following reasons (Fig. 6 and Table 1): (i) as described in the previous section, mtInhA inhibition was moderate but improved by the introduce of methyl and ethyl groups (compounds **3d** and **3f**); (ii) mtInhA inhibitory activity by the derivatives with the *tert*-butyl groups (compounds **3b** and **3g**) were comparable to that of KES4; (iii) in spite of trifluorometyl group is *tert*-butyl derivative, compound **3e** inhibited 55% of the enzymatic activity. These observations suggested that the space around KES4 A-ring observed in mtInhA binding cavity (see Fig. 1b) could be buried by small and hydrophobic substituents and the interaction with the enzyme could be facilitated, while bulky substituents hindered the interaction.

Compounds **3d** and **3f** showed preferable features in terms of antimycobacterial activity, cytotoxicity toward mammalian cells, inhibitory activity against mtInhA, and antibacterial effects on *Escherichia coli* as indigenous model bacteria. The properties of KES4 as antimycobacterial

Table 1 Effect on mtInhA activity and lipophilicity (tPSA and Log*P*) of the compounds

Compounds	mtInhA activity (%)[a]	tPSA	Log*P*
DMSO	100 ± 3.1	–	–
KES4	68.0 ± 0.5	47.1	2.88
3a	83.4 ± 1.2	73.4	2.59
3b	63.9 ± 0.7	47.1	4.18
3c	48.8 ± 2.4	47.1	4.34
3d	39.5 ± 0.6	47.1	3.44
3e	45.4 ± 1.2	47.1	4.21
3f	41.2 ± 0.6	47.1	4.18
3g	66.5 ± 2.1	47.1	2.88

[a]MtInhA (0.7 μM) was preincubated with each compound (50 μM) at room temperature for 1 min before its activity was measured. Vehicle (0.3% DMSO) was used as the negative control. All experiments were performed in triplicate, and data are expressed as mean ± SD

agents might be improved by introduction of small alkyl groups (e.g., ethyl, methyl) to the A-ring. Nevertheless, the KES derivatives excepting compound **3a** showed severe growth inhibitions of *M. smegmatis* (Figs. 3 and 4), whereas these compounds showed only moderate activity on mtInhA inhibition (Fig. 6). These IC_{50} values were estimated as 1.8–22.8 μM, though the enzymatic activity was inhibited <50% under the presence of 50 μM of each compound. These observations and discrepancy imply that KES4 and its derivatives could inhibit other lethal targets in Mycobacterium. As another possibility, metabolites from KES4 and its derivatives might exert InhA inhibitory effect.

In summary, we constructed virtual compound library of A-ring-modified KES4 compounds using commercially available phenol derivatives as building blocks for the A-ring. We succeeded in synthesizing seven KES4 derivatives (compounds **3a**–**g**) from 16 candidates (KET1-16), which were identified by in silico docking simulation. Two candidates (compounds **3d** and **3f**) exhibited superior properties to KES4 as mtInhA-targeted anti-infectives for mycobacteria. Together, present study demonstrated that custom-made compound library screening combined with organic synthesis could be a cost- and labor-saving technique for the improvement of lead compounds. Experimental validation of bioactivity should also be necessary not only for acquisition of compounds with preferable bioactivities, but also for the SAR study.

Acknowledgements This work was supported in part by a Takeda Science Foundation to JT, and a Grant-in-Aid for Scientific Research (C) (26460145) to SA and (18K05358) to HS from the Ministry of Education, Culture, Sports, Science, and Technology of Japan.

Compliance with ethical standards

Conflict of interest The authors declare that they have no conflict of interest.

References

1. Dye C, Williams BG. The population dynamics and control of tuberculosis. Science. 2010;328:856–61.
2. Das P, Horton R. Tuberculosis-time to accelerate progress. Lancet. 2010;375:1755–7.
3. Das P, Horton R. Tuberculosis-getting to zero. Lancet. 2015;386:2231–2.
4. Lönnroth K, Castro KG, Chakaya JM, Chauhan LS, Floyd K, Glaziou P, et al. Tuberculosis control and elimination 2010-50: cure, care, and social development. Lancet. 2010;375:1814–29.
5. Sotgiu G, Centis R, D'Ambrosio L, Migliori GB. Tuberculosis treatment and drug regimens. Cold Spring Harb Perspect Med. 2015;5:a017822.
6. Banerjee A, Dubnau E, Quemard A, Balasubramanian V, Um KS, Wilson T, et al. InhA, a gene encoding a target for isoniazid and ethionamide in *Mycobacterium tuberculosis*. Science. 1994;263:227–30.
7. Parikh SL, Xiao G, Tonge PJ. Inhibition of InhA, the enoyl reductase from *Mycobacterium tuberculosis*, by triclosan and isoniazid. Biochemistry. 2000;39:7645–50.
8. McMurry LM, McDermott PF, Levy SB. Genetic evidence that InhA of Mycobacterium smegmatis is a target for triclosan. Antimicrob Agents Chemother. 1999;43:711–3.
9. Quemard A, Sacchettini JC, Dessen A, Vilcheze C, Bittman R, Jacobs WR Jr, et al. Enzymatic characterization of the target for isoniazid in *Mycobacterium tuberculosis*. Biochemistry. 1995;34:8235–41.
10. Brennan PJ, Nikaido H. The envelope of mycobacteria. Annu Rev Biochem. 1995;64:29–63.
11. Tonge PJ, Kisker C, Slayden RA. Development of modern InhA inhibitors to combat drug resistant strains of *Mycobacterium tuberculosis*. Curr Top Med Chem. 2007;7:489–98.
12. Rotta M, Pissinate K, Villela AD, Back DF, Timmers LF, et al. Piperazine derivatives: synthesis, inhibition of the *Mycobacterium tuberculosis* enoyl-acyl carrier protein reductase and SAR studies. Eur J Med Chem. 2015;90:36–447.
13. Vilcheze C, Morbidoni HR, Weisbrod TR, Iwamoto H, Kuo M, et al. Inactivation of the inhA-encoded fatty acid synthase II (FASII) enoyl-acyl carrier protein reductase induces accumulation of the FASI end products and cell lysis of *Mycobacterium smegmatis*. J Bacteriol. 2000;182:59–4067.
14. Oliveira JS, Pereira JH, Canduri F, Rodrigues NC, de Souza ON, de Azevedo WF Jr, et al. Crystallographic and pre-steady-state kinetics studies on binding of NADH to wild-type and isoniazid-resistant enoyl-ACP(CoA) reductase enzymes from *Mycobacterium tuberculosis*. J Mol Biol. 2006;359:646–66.
15. Taira J, Ito T, Nakatani H, Umei T, Baba H, Kawashima S, et al. In silico structure-based drug screening of novel antimycobacterial pharmacophores by DOCK-GOLD tandem screening. Int J Mycobacteriol. 2017;6:142–8.
16. Taira J, Morita K, Kawashima S, Umei T, Baba H, Maruoka T, et al. Identification of a novel class of small compounds with anti-tuberculosis activity by in silico structure-based drug screening. J Antibiot. 2017;70:1057–64.
17. Kinjo T, Koseki Y, Kobayashi M, Yamada A, Morita K, Yamaguchi K, et al. Identification of compounds with potential antibacterial activity against Mycobacterium through structure-based drug screening. J Chem Inf Model. 2013;53:1200–12.
18. Koseki Y, Kinjo T, Kobayashi M, Aoki S. Identification of novel antimycobacterial chemical agents through the in silico multi-conformational structure-based drug screening of a large-scale chemical library. Eur J Med Chem. 2013;60:333–39.
19. Kanetaka H, Koseki Y, Taira J, Umei T, Komatsu H, Sakamoto H, et al. Discovery of InhA inhibitors with anti-mycobacterial activity through a matched molecular pair approach. Eur J Med Chem. 2015;94:378–85.
20. He X, Alian A, Stroud R, Ortiz, de Montellano PR. Pyrrolidine carboxamides as a novel class of inhibitors of enoyl acyl carrier protein reductase from *Mycobacterium tuberculosis*. J Med Chem. 2006;49:6308–23.
21. Kobayashi M, Kinjo T, Koseki Y, Bourne CR, Barrow WW, Aoki S. Identification of novel potential antibiotics against Staphylococcus using structure-based drug screening targeting dihydrofolate reductase. J Chem Inf Model. 2014;54:1242–53.
22. Koseki Y, Aoki S. Computational medicinal chemistry for rational drug design: Identification of novel chemical structures with potential anti-tuberculosis activity. Curr Top Med Chem. 2014;14:176–88.

23. Schmidt CW. TOX 21: new dimensions of toxicity testing. Environ Health Perspect. 2009;117:A348.
24. Faulon JL, Visco DP, Pophale RS. The signature molecular descriptor. 1. Using extended valence sequences in QSAR and QSPR studies. J Chem Info Comput Sci. 2003;43:707–20.
25. Berenger F. MolEnc: a molecular encoder using rdkit and OCaml. 2019. https://github.com/UnixJunkie/molenc. Accessed 19 Nov 2019.
26. Breiman L. Bagging predictors. Mach Learn. 1996;24:123–40.
27. Platt J. Probabilistic outputs for support vector machines and comparisons to regularized likelihood methods. Adv Large Margin Classif. 1999;10:61–74.
28. Molle V, Gulten G, Vilcheze C, Veyron-Churlet R, Zanella-Cleon I, Sacchettini JC, et al. Phosphorylation of InhA inhibits mycolic acid biosynthesis and growth of Mycobacterium tuberculosis. Mol Microbiol. 2010;78:1591–605.
29. Delaine T, Bernardes-Génisson V, Quémard A, Constant P, Meunier B, et al. Development of isoniazide NAD truncated adducts embedding a lipophilic fragment as potential bi-substrate InhA inhibitors and antimycobacterial agents. Eur J Med Chem. 2010;45:4554–61.
30. Jones G, Willett P, Glen RC. Molecular recognition of receptor sites using a genetic algorithm with a description of desolvation. J Mol Biol. 1995;245:43–53.
31. Jones G, Willett P, Glen RC, Leach AR, Taylor R. Development and validation of a genetic algorithm for flexible docking. J Mol Biol. 1997;267:727–48.